

University of Dundee

Passivating effect of ternary alloyed AgZnSe shell layer on the structural and luminescent properties of CdS quantum dots

Adegoke, Oluwasesan; Montaseri, Hanieh; Nsibande, Sifiso A.; Forbes, Patricia B.C.

Published in:
Materials Science in Semiconductor Processing

DOI:
[10.1016/j.mssp.2018.10.025](https://doi.org/10.1016/j.mssp.2018.10.025)

Publication date:
2019

Licence:
CC BY-NC-ND

Document Version
Peer reviewed version

[Link to publication in Discovery Research Portal](#)

Citation for published version (APA):

Adegoke, O., Montaseri, H., Nsibande, S. A., & Forbes, P. B. C. (2019). Passivating effect of ternary alloyed AgZnSe shell layer on the structural and luminescent properties of CdS quantum dots. *Materials Science in Semiconductor Processing*, 90, 162-170. <https://doi.org/10.1016/j.mssp.2018.10.025>

General rights

Copyright and moral rights for the publications made accessible in Discovery Research Portal are retained by the authors and/or other copyright owners and it is a condition of accessing publications that users recognise and abide by the legal requirements associated with these rights.

Take down policy

If you believe that this document breaches copyright please contact us providing details, and we will remove access to the work immediately and investigate your claim.

1 **Passivating effect of ternary alloyed AgZnSe shell layer on the**
2 **structural and luminescent properties of CdS quantum dots**

3

4 Oluwasesan Adegoke, Hanieh Montaseri, Sifiso A. Nsibande, Patricia B.C. Forbes *

5 *Department of Chemistry, Faculty of Natural and Agricultural Sciences, University of Pretoria,*
6 *Lynnwood Road, Pretoria 0002, South Africa*

7

8

9

10

11

12

13

14

15

16

17

18

19

20

21 *Corresponding author: *Email address:* adegoke.sesan@mailbox.co.za (O. Adegoke),

22 patricia.forbes@up.ac.za (P.B.C. Forbes)

23 **Abstract**

24 The surface passivation of luminescent CdS quantum dots (QDs) via epitaxial overgrowth of new
25 alloyed ternary AgZnSe shell layer is reported here. Two synthetic fabrication strategies were used
26 to tune the optical properties of CdS/AgZnSe core/alloyed shell QDs across the visible region.
27 Transmission electron microscopy, powder X-ray diffraction, Raman, UV/vis and fluorescence
28 spectrophotometric techniques were used to characterize the nanocrystals. Analysis of the internal
29 structure of the QDs revealed that homogeneity of the particle reduced as the size increased, thus
30 indicating that the QDs growth transitioned from an interfacial epitaxial homogenous state to a
31 heterogeneous state. The crystal structure of the QDs revealed a distinct zinc-blende diffraction
32 pattern for CdS while CdS/AgZnSe core/alloyed shell QDs kinetically favoured a phase change
33 process from the zinc-blende phase to a wurtzite phase. Analysis of the photophysical properties
34 revealed varying degrees of interfacial defect state suppression in CdS/AgZnSe QDs which was
35 dependent on the QDs size. Specifically, the fluorescence quantum yield (QY) of CdS/AgZnSe
36 QDs was at most ~5-fold higher than the CdS core and varied from 35-73%. We found that band
37 gap modulation via the synthetic fabrication strategy employed, influenced the optical properties
38 of the core/alloyed shell QDs. The CdS/AgZnSe QDs produced in this work hold great promise in
39 light-emitting optoelectronic applications.

40

41

42 *KEYWORD:* Quantum dots; surface defects; photoluminescence; quantum yield; alloyed

43

44

45

46

47 **1. Introduction**

48 The wide electro-luminescent applications of colloidal semiconductor quantum dot (QD)
49 nanocrystals in various fields of chemistry, biology and physics, stem from their unique
50 optoelectronic properties [1,2]. Particularly, the size-dependent optical and electronic properties
51 of QDs which are governed by the associated quantum confinement feature, allows tuning of the
52 photoluminescence (PL) emission from the ultraviolet/visible (UV/vis) region to the far infra-red
53 region [3-6]. In contrast to bulk semiconductors in which the surface represents a tiny fraction of
54 the bulk material, colloidal QDs have their size typically in the range of 2–10 nm. This unique
55 characteristic enables a large number of atoms to be embedded on the QD surface [7].

56 The QD surface represents a highly sensitive region that is exposed to its surrounding environment
57 (matrices, solvents and various other species in solution) and it is typically coordinated by
58 chemical ligands, surfactants or stabilizers that influence the QD optoelectronic properties [7]. The
59 synergistic effects of precursor material which create low numbers of coordinated surface atoms
60 may lead to highly reactive or localized electronic sites that are susceptible to redox and chemical
61 processes. Thus, it is very likely for midgap, shallow or deep surface defect states to be formed
62 and induce the pathway for poor PL properties. The characteristic phenomenon is nonradiative
63 recombination exciton (electron and hole) states associated with low PL quantum yield (QY) [8,9].

64 One of the widely used strategies to eliminate surface traps is to passivate the QD core surface
65 with a wider band gap shell material [10-13]. This strategy shifts the surface defects to the outer
66 domain of the shell layer, thus improving the PL QY [4]. The electron and hole being localized in
67 the core, represents a signature process associated with the low probability of the outer surface
68 state being subjected to trapped photogenerated charge carriers [14,15].

69 Over the past two decades, the most studied class of semiconductor QDs are the group II-VI metal
70 chalcogenides with CdSe-based QDs being the most popular for fabricating new synthetic routes
71 [16], shell passivation [17], ligand dynamics [18] and alloying [19]. On the other hand, CdS
72 nanocrystals are probably the second most studied QD system [20-23], exhibiting an exciton Bohr
73 radius of 3.0 nm [24] and a bulk band gap of 2.48 eV [25]. Its characteristic PL emission is known
74 to be highly prone to surface defects which results in low PL QY [26]. Nonetheless, it is widely
75 used as a shell layer to overcoat the surface of CdSe-based QDs. The well-known strategy to isolate
76 the exciton wave function from the surface of the core QDs with embedded surface defects and
77 dangling bonds is to coat with a shell layer of a wide band gap [27]. However, it is important to
78 note that lattice mismatch between the core and binary shell material at the interface can also
79 induce surface defects that degrade the luminescence of the core/shell QDs, thus lowering the PL
80 QY [28].

81 Another strategy which has drawn significant interest in improving the PL QY of binary core QDs
82 is to coat the surface with an alloyed ternary shell layer. Alloyed QDs (AB_xC_{1-x}) have become
83 important in mainstream nanoscale optical engineering due to the added degree of freedom in
84 tuning the exciton energy for either extended PL emission range or improved optical properties
85 [29-32]. The coating of an alloyed ternary shell around binary core QDs to improve the PL
86 efficiency has mostly been reported for CdSe-based QDs [33,34] with rare reports for CdS-based
87 QDs [13]. It is noteworthy that apart from the formation of a smooth gradient band gap, the lattice
88 strain of the core/shell QDs can be relaxed due to alloying [35]. Furthermore, it has been
89 demonstrated that shell alloying suppressed Auger exciton recombination in core/alloyed shell/
90 shell QDs, thus increasing the PL QY [36].

91 Overcoating a shell layer around the CdS core to improve the PL QY of QDs has rarely been
92 studied. Thus, in this paper, we report on a new strategy to suppress the surface defect states of
93 CdS QDs by coating with a new ternary alloyed shell layer. CdS QDs, characterized by low PL
94 QY due to embedded surface defects were synthesized in this work via the organometallic
95 synthetic route. We have demonstrated for the first time that improved PL QY in CdS QDs can be
96 achieved via passivation with a ternary alloyed AgZnSe shell layer. To the best of our knowledge,
97 our work is the first to overcoat a AgZnSe shell around CdS core QDs with the sole aim of
98 suppressing interfacial defect states in the core QDs. The organic-phase CdS/AgZnSe core/alloyed
99 shell QDs produced in this work hold great promise in light-emitting optoelectronic applications.

100

101 **2. Experimental section**

102 *2.1. Materials*

103 Cadmium oxide (CdO), myristic acid, trioctylphosphine oxide (TOPO), hexadecylamine (HDA),
104 trioctylphosphine (TOP), octadecene (ODE), oleic acid, sulphur (S), L-cysteine, diethylzinc
105 (Et_2Zn) and zinc oxide (ZnO) were purchased from Sigma Aldrich. Silver nitrate (AgNO_3) was
106 purchased from Saarchem. Selenium (Se) was purchased from Merck. Methanol, acetone, hexane
107 and chloroform were purchased from ACE Chemicals.

108

109 *2.2. Characterization*

110 UV/vis absorption spectra were obtained using a Cary Eclipse (Varian) spectrophotometer. PL
111 emission measurements were carried out using a Horiba Jobin Yvon Fluoromax-4
112 spectrofluorometer. Powder X-ray diffraction (PXRD) measurements were determined using a
113 $\text{Cu}(\text{K}\alpha)$ radiation ($\lambda=1.54184 \text{ \AA}$) on a Bruker D2 Phaser. Transmission electron microscopy (TEM)

114 images were produced using a JEOL JEM 2100F operated at 200 kV. Raman spectra were recorded
115 using a WITec Alpha 300 micro-Raman imaging system with a 488 nm excitation laser and CCD
116 detector at ambient temperature with the laser power below 2 mW in order to reduce heating
117 effects.

118

119 *2.3. Preparation of the precursors*

120 *2.3.1. TOPSe*

121 To prepare the Se precursor, 0.12 g Se was dissolved in 5 mL TOP and sonicated until complete
122 dissolution of Se, thus resulting in a clear solution. The solution was then stirred at room
123 temperature prior to use and was stable for 3 days.

124

125 *2.3.2. TOPZn*

126 To prepare the Zn precursor from Et_2Zn , 1.93 g TOPO was firstly dissolved in 10 mL ODE and 5
127 mL of oleic acid. The solution was then heated up until the complete dissolution of TOPO
128 surfactant, thus resulting in a clear solution. Thereafter, 2 mL Et_2Zn and 1 mL TOP were added
129 and the solution was stirred at room temperature before use.

130 To prepare the Zn precursor from ZnO, 0.4 g ZnO was added to a mixture of 15 mL ODE and 10
131 mL oleic acid and sonicated for a few minutes. Thereafter, the precursor solution was stirred at
132 room temperature prior to use.

133

134 *2.3.3. TOPAg*

135 Ag precursor was prepared by mixing 0.5 g AgNO₃ with 5 mL TOP. The solution was then heated
136 up until complete dissolution of the AgNO₃ which was evident by the change in colour from
137 colourless to brownish black.

138 2.3.4. TOPS

139 To prepare the TOPS precursor used in method 1 synthesis of CdS/AgZnSe QDs (refer to section
140 2.4), 1.93 g TOPO was first dissolved in 15 mL ODE and 10 mL oleic acid followed by the addition
141 of 0.16g S and 1 mL TOP. For method 2 synthesis of CdS/AgZnSe QDs (section 2.5), 1.93 g
142 TOPO was dissolved in 10 mL ODE and 5 mL oleic acid, then 0.08 g S and 1 mL TOP was added
143 thereafter. The solutions were sonicated and heated up to aid complete dissolution of the S and
144 thereafter stirred at room temperature prior to use.

145

146 2.4. Synthesis of CdS/AgZnSe core/alloyed shell QDs (method 1)

147 The synthesis of CdS/AgZnSe core/alloyed shell QDs was carried out via the organometallic one-
148 pot synthetic route but with modifications [37]. Complexation between the Cd ion, surfactants
149 and capping ligands was formed by mixing 1.3 g CdO, 1.2 g myristic acid, 1.93 g TOPO and 1.2
150 g HDA with 50 mL ODE and 30 mL of oleic acid. The solution was bubbled with Ar gas and
151 heated up until complete dissolution of the Cd ion which was evident by a change in colour of the
152 solution from pale brown to colourless. At ~220 °C, TOPS solution was added into the Cd
153 precursor solution to form the CdS core QDs. Once satisfactory growth of the QD core was
154 achieved, a fraction of the growth solution was injected into a beaker. To form the core/alloyed
155 shell QDs, 1 ml of TOPSe solution was added into the CdS growth solution followed swiftly by
156 the addition of 1 mL TOPAg and TOPZn (using ZnO). Portions of the core/shell QDs were taken
157 out at different time intervals.

158 2.5. Synthesis of CdS/AgZnSe QDs (method 2)

159 Method 2 synthesis was carried out according to the fabrication steps detailed in method 1 but with
160 slight modifications of the precursor concentrations. For the complexation of Cd ion with the
161 precursor materials, 2 mL TOP, 0.4 g CdO, 0.6 g HDA and 0.6 g myristic acid were mixed with
162 20 mL ODE and 15 mL oleic acid. The synthetic process of method 1 was thereafter followed by
163 adding TOPS (prepared specifically for method 2) to form the CdS QDs. Formation of the
164 core/alloyed shell QDs was followed according to method 1 except that TOPZn prepared from
165 Et_2Zn was used.

166

167 **3. Results and discussion**

168 *3.1. Fabrication of the QDs*

169 One-pot organometallic synthesis of metal precursors in the presence of surfactants, organic-
170 capping ligands and a non-coordinating solvent (ODE) was used to engineer the structure of the
171 QDs. It is well known that the growth kinetics influences the PL emission and absorption evolution
172 of the QDs [38]. The nature of the precursor material with respect to the concentration, quantity,
173 time of injection, temperature and the interplay between them are reaction conditions that influence
174 the growth of the QDs. We have therefore exploited these reaction conditions to engineer the
175 optical properties of CdS/AgZnSe core/alloyed shell QDs.

176 In method 1 synthesis, higher quantities of the Cd metal precursor, surfactants, organic ligands and
177 the non-coordinating solvent were used to aid the Cd-precursor complexation for the subsequent
178 nucleation and growth of CdS QDs. Conversely, lower concentrations of the Cd precursor,
179 surfactants and ligands were employed in method 2 synthesis of the QDs. Before adding the TOPS
180 precursor, the Cd precursor solution was heated up to $>200\text{ }^\circ\text{C}$ to aid complete dissolution and

181 complexation of the Cd precursor. The change in colour of the solution from brown to colourless
182 confirmed the complexation process which was accompanied by injection of the TOPS precursor.
183 As the CdS core QDs nucleated, the temperature of the growth solution increased steadily and was
184 accompanied by a concomitant change in the colour. During this period, a fraction of the CdS core
185 QDs was removed in order to probe the structural and optical properties thereof in comparison to
186 the core/alloyed shell QDs.

187 The temperature at which the AgZnSe alloyed shell was overcoated on the CdS core surface is
188 very crucial to the overall optical properties of the CdS/AgZnSe core/alloyed shell QDs. At higher
189 temperature and longer reaction time, CdS QDs size distribution is expected to deteriorate and lead
190 to broadening of the spectral line widths. On the other hand, overcoating the shell layer at relatively
191 low temperature could either reduce the crystallinity of CdS/AgZnSe core/alloyed shell QDs or
192 lead to incomplete decomposition of the precursor materials [39]. Therefore, an appropriate
193 temperature was determined independently for each method used to fabricate the core/alloyed shell
194 QDs. The concentration and rate at which the AgZnSe shell precursor is added is also crucial in
195 influencing the optical properties of the QDs. Slow addition of the precursor shell materials
196 prevents homogenous nucleation and induces most of the AgZnSe shell to grow heterogeneously
197 on the CdS nuclei. Hence, the precursor solutions for the shell layering were injected into the CdS
198 growth solution in swift succession. Addition of TOPSe, TOPZn and TOPAg precursors to the
199 CdS growth solution triggered a progressive change in the colour of the solution from orange to
200 red and to dark brown. Different sizes of the CdS/AgZnSe QDs were thereafter harvested at
201 different time intervals whilst the QDs were purified with acetone, chloroform/acetone and
202 chloroform/acetone/ethanol mixture.

203

204 *3.2. Structural properties*

205 *3.2.1. Surface morphology*

206 TEM analysis was used to qualitatively probe the internal structure of the QDs with respect to the
207 shape, size distribution, and shell coverage. Fig. 1A-C shows the TEM images of three different-
208 sized CdS QDs with average sizes of 6.0 ± 0.5 , 6.5 ± 0.5 and 7.5 ± 1.2 nm respectively. Our aim was
209 to synthesize uniform-sized CdS QDs in order to effectively understand the structural effects of
210 shell layering. Looking closely at each TEM micrograph, a uniform size distribution, embedded
211 with a mixture of spherical and quasi-spherical shapes was observed. Thus, the monodispersed
212 particle size distribution provides direct indication of homogenous nucleation and growth of the
213 core QDs.

214 Alloyed semiconductor QD nanocrystals can be grouped as having either a gradient internal
215 structure derived from varying the alloy composition or a uniform internal structure ascribed to
216 homogenous alloying. In our work, a fixed composition of the shell precursor was used to engineer
217 the structure of the core/alloyed shell QDs. Fig. 2A-D shows the representative TEM images of
218 CdS/AgZnSe core/alloyed shell QDs synthesized via method 1 with average particle sizes of
219 5.1 ± 0.6 , 5.5 ± 0.7 , 7.9 ± 1.6 and 9.1 ± 1.9 nm respectively. The striking feature was the decrease in
220 the core/alloyed shell QDs particle size relative to the core which is an unusual phenomenon as
221 the size of the core/shell QDs is expected to increase after shell passivation. Since shell passivation
222 of the 7.5 nm CdS QDs led to rapid nucleation and growth of the different sized CdS/AgZnSe
223 QDs, it is imperative to suggest that either CdS was buried within the shell domain or an
224 intermediate formation of CdS/CdSe occurred before the growth of CdS/AgZnSe QDs.

225 As the CdS/AgZnSe QDs grew, a steady transformation in the particle morphology with respect
226 to the size distribution was observed. The homogeneity of the particle reduced as the size

227 increased, thus indicating that the QDs growth transitioned from an interfacial epitaxial
228 homogenous state to a heterogeneous state. During the period of harvesting each of the different-
229 sized QDs, the temperature of the solution increased from ~240 – 310 °C and this should
230 tentatively influence the nucleation and growth of the QDs. It is also noteworthy to emphasize that
231 the transition in homogeneity of the QDs correlated significantly to the shape engineering of the
232 particle. Looking closely at the TEM monograph of 7.9 nm and 9.1 nm-sized CdS/AgZnSe QDs
233 (Fig. 2C and 2D), the emergence of trigonal-shaped particles was observed. Tentatively, we could
234 attribute the shape engineering of the QDs to the passivating effect of AgZnSe shell, thus implying
235 that the electronic structure of CdS/AgZnSe QDs led to different confinement levels for electron
236 and hole. The hole may be strongly confined to the CdS core while the electron may be delocalised
237 into the shell layer [40].

238 Three different sizes of CdS/AgZnSe QDs were harvested using method 2 synthetic route. The
239 corresponding TEM images and particle size histograms are shown in Fig. 3. The particle size
240 distribution revealed a prolate heterogeneous particle morphology, resembling an anisotropic-like
241 growth pattern. The anisotropic growth pattern can be understood in terms of the reaction
242 conditions used in the synthesis as it applies to low reactivity precursors and low volume of
243 coordinating solvent. Under these reaction conditions, CdS/AgZnSe heteroepitaxial growth is
244 kinetically controlled (i.e., AgZnSe formation at the surface is the rate-limiting step, rather than
245 the precursor diffusion) and slow. Thus, the high reactivity of the Ag, Zn and Se of the AgZnSe
246 shell layer will favour anisotropic-type growth [41].

247 Generally, the mechanism of nucleation and growth of CdS/AgZnSe QDs can be understood in
248 terms of Ostwald ripening. At relatively low temperature (220–240 °C), Ostwald ripening
249 dominated as a result of dissolution and surface energy of small particles which redissolve to allow

250 subsequent growth of larger particles. At higher temperature ($>260\text{ }^{\circ}\text{C}$), Brownian motion will
251 increase in the synthetic system due to higher thermal energy. Hence it is more likely that the
252 increase in motion will allow the particles to interact at the exact crystallographic orientation,
253 leading to orientated attachment [42].

254

255 3.2.2. Crystal phase analysis

256 The crystal structure of CdS core and CdS/AgZnSe QDs was studied using PXRD. From the
257 diffraction pattern of the CdS core (Fig 4), a pure zinc-blende crystal structure with three prominent
258 peaks at planes {111}, {220} and {311} was observed. The three planes exhibited Bragg angles
259 at 26.5° , 43.9° and 51.9° respectively. Comparison of the diffraction pattern of CdS/AgZnSe
260 core/alloyed shell QDs with CdS QDs reveal notable differences. Firstly, the three-notable peaks
261 (associated with zinc-blende crystal structure) present in CdS were observed in CdS/AgZnSe₅₈₈.
262 However, the appearance of four additional peaks between $30\text{--}40^{\circ}$ and two additional peaks at
263 higher Bragg angle (47.6° and 56.8°) provides direct evidence that the shell alloying process
264 induced crystal phase changes in the QDs. Since the CdS/AgZnSe QDs size was tuned by fixed
265 shell alloying, it is interesting to note the phase transition changes in the core/alloyed shell QDs.
266 As the size of CdS/AgZnSe QDs increased, a steady transformation in the diffraction pattern as it
267 relates to changes in the diffraction peaks was observed. A close assessment of the diffraction
268 pattern of CdS/AgZnSe₅₉₃, revealed detailed formation of a duplet peak at low Bragg angle which
269 can be attributed to the steady phase transition from a zinc-blende diffraction pattern to a wurtzite
270 diffraction pattern. Further growth of the core/alloyed shell QDs led to the formation of a triplet
271 peak at low angle as observed from the diffraction pattern of CdS/AgZnSe₅₉₉. Further assessment
272 of the diffraction pattern of CdS/AgZnSe₆₀₁ revealed the formation of a pure wurtzite diffraction

273 pattern. Thus, it can be concluded that CdS core QDs favoured a zinc-blende crystal structure
274 while the CdS/AgZnSe core-alloyed QDs kinetically favoured a phase change from a zinc-blende
275 diffraction pattern to a wurtzite diffraction pattern.

276

277 3.2.3. Raman analysis

278 Core/shell QDs have been proven to reduce Auger recombination rates, which is important in
279 multiexciton recombination and OFF/ON blinking process [43]. It is also believed that the
280 core/shell interfacial alloying region is associated with a graded interface [44]. Hence, the potential
281 of Raman to probe the internal structure of the core/alloyed shell QDs interface was investigated.
282 Fig. 5 shows the Raman spectra for CdS core and the different-sized CdS/AgZnSe QDs. The
283 similarities with reference to the peak position of CdS longitudinal optical phonon (LO) bulk
284 frequency at $\sim 300 \text{ cm}^{-1}$ and CdS overtone at $\sim 600 \text{ cm}^{-1}$ with those of CdS/AgZnSe₅₈₈ and
285 CdS/AgZnSe₉₃, provides strong indication of the homogenous growth of the core/alloyed shell
286 QDs. For CdS/AgZnSe₅₉₉ and CdS/AgZnSe₆₀₁, we observed significant changes in the peak
287 position when compared to the CdS core. Specifically, the peak position of CdS/AgZnSe₅₉₉
288 exhibited similar frequency to CdS LO frequency but the peak at the CdS overtone region was
289 more blue-shifted in frequency. Conversely, the peak frequencies of CdS/AgZnSe₅₉₉ relative to
290 CdS LO and the overtone region were more red-shifted in comparison to the CdS core. The degree
291 of frequency shift in CdS/AgZnSe₅₉₉ and CdS/AgZnSe₆₀₁ peak position relative to CdS can be
292 understood in terms of the growth morphology and the degree of interfacial defect states in the
293 QDs. Thus, the frequency shift and strain relaxation in the core/alloyed shell interface will differ
294 due to the QDs size and shell thickness. The relatively less-pronounced peaks below 220 cm^{-1} for
295 the core/alloyed shell QDs can be ascribed to a surface optical phonon feature which is inherent in

296 finite sized crystals and also from the varying degree of alloying at the interface between CdS core
297 and AgZnSe shell [45,46]. The variation in the intensity of the modes below 220 cm⁻¹ could
298 probably also account for the differences in alloying efficiency of the AgZnSe shell relative to the
299 CdS core.

300

301 3.3. Optical properties

302 The QDs surface is influenced by the nature and chemical reaction of the synthetic constituents
303 (surfactants, capping ligands and solvents) used in fabricating its structure. The atomistic effects
304 of these constituents form the basis for assessing the quality of the QDs surface as it relates to the
305 optical properties, such as the PL stability, spectral features and PL QY. The formation of midgap,
306 deep and shallow states as surface traps provides the basis to which nonradiative electron-hole
307 recombination degrades the QDs fluorescence. The suppression or total elimination of surface trap
308 states in core QDs via coating of a shell layer is useful for light-associated applications and it
309 provides a platform for better understanding of synthetic fabrication strategies required to
310 construct high-quality QD nanocrystals. Our objective is to investigate the influence of a new shell
311 layer (AgZnSe) on the luminescent properties of colloidal CdS QDs. We have utilized the shell
312 alloying process to unravel how the QDs band gap and synthetic fabrication strategy influences
313 the PL properties of CdS/AgZnSe core/alloyed shell QDs. The PL QY was determined according
314 to the equation:

315

$$316 \quad \Phi_F^{QD} = \Phi_F^{Std} \frac{F_{QDs} \cdot OD_{Std}(\lambda_{exc}) \cdot n_{water}^2}{F_{Std} \cdot OD_{QD}(\lambda_{exc}) \cdot n_{ethanol}^2} \quad (1)$$

317

318 Where $\Phi_{\text{F}}^{\text{Std}}$ is the PL quantum yield of rhodamine 6G standard in ethanol ($\Phi = 0.95$); F_{Std} and F_{QDs}
319 are the integrated sum of the fluorescence intensity of the standard and QDs; $\text{OD}_{\text{QD}(\lambda_{\text{exc}})}$ and $\text{OD}_{\text{Std}(\lambda_{\text{exc}})}$
320 are the optical densities of the QDs and standard while n_{ethanol}^2 and n_{water}^2 are the refractive indices of
321 ethanol and water used to prepare the standard and QDs respectively.

322 Fig. 6A and B shows the evolution of the PL emission and absorption spectra of three different-
323 sized CdS core QDs and Table 1 summarizes the corresponding photophysical properties as they
324 relate to the absorption wavelength maximum, full width at half maximum (FWHM), band gap
325 and PL QY. We harvested three-sized CdS core QDs with the sole aim of assessing their optical
326 properties in comparison to the different-sized CdS/AgZnSe core/alloyed shell QDs. A small red
327 shift in PL emission was observed for the harvested different-sized CdS core QDs with the
328 absorption wavelength maximum and FWHM increasing in relation to the core size. The striking
329 feature is the low PL QY which was increasingly tuned from 4 to 16% and also dependent on each
330 core size. We observed that CdS₄₇₁ produced the highest PL QY of 16% while the lowest PL QY
331 value of 4% was exhibited by CdS₄₇₈. Based on the relatively low PL QY, CdS core QDs suffers
332 significantly from interfacial surface defects and residual strain in which the degree of defect states
333 depends on the core size.

334 To effectively understand the effect of ternary AgZnSe shell alloying on the PL properties of CdS
335 QDs, we employed two synthetic fabrication strategies. The most obvious and direct evidence of
336 shell alloying comes from the PL emission and absorption spectra shown in Fig. 6C. The evolution
337 of the PL emission of CdS/AgZnSe QDs synthesized via method 1 was tuned from 588 to 601 nm
338 while the absorption spectra (Fig. 6D) was tuned from 464 nm to 477 nm. AgZnSe shell precursors
339 used in method 1 synthesis of CdS/AgZnSe QDs was added into the growth solution after
340 harvesting fraction of CdS₄₈₁ core QDs. The striking feature is the blue-shifted absorption

341 wavelength and corresponding red shift in PL emission of CdS/AgZnSe₅₈₈ relative to CdS₄₈₁ QDs.
342 The shift reveals that the shell alloying strategy, induced band gap modulation of the QDs in the
343 visible region of the electromagnetic spectrum. For CdS/AgZnSe QDs synthesized via method 2,
344 the PL emission spectra was tuned from 591 to 612 nm (Fig. 7A) while the absorption spectra were
345 tuned from 449 to 481 (Fig. 7B). Despite the PL emission being more red-shifted relative to the
346 CdS core, the absorption spectrum of CdS/AgZnSe₅₉₁ was significantly blue-shifted. From Table
347 1, the efficiency of band gap modulation of CdS/AgZnSe QDs was observed to vary narrowly
348 from 2.07–2.11 eV for method 1 synthesis and from 2.03–2.10 eV for method 2 synthesis of the
349 QDs.

350 To determine if the band gap modulation of CdS/AgZnSe QDs originated from the intrinsic optical
351 properties of the core/alloyed nanostructures, a deeper assessment of the PL QY values (Table 1)
352 was performed. The most striking observation is the variation in the PL QY of CdS/AgZnSe QDs
353 synthesized via method 1 and 2 and the remarkable increase in comparison to the values obtained
354 for CdS core. Via method 1 synthesis, the PL QY of CdS/AgZnSe QDs was tuned from 48 to 51%
355 but via method 2 synthesis the PL QY was tuned from 35 to 73%. It is noteworthy that shell
356 alloying of CdS QDs suppressed interfacial defect states in the core/alloyed shell nanocrystals due
357 to the remarkable increase in the PL QY. However, it is important to emphasize that the defect
358 state suppression efficiency varied amongst the QDs size and was dependent on the quality of the
359 fabrication method.

360 Examining closely how the shell alloying process influenced the optical properties of the QDs, we
361 have probed the correlation between the band gap modulation and the PL QY. It is a well-
362 established phenomenon that a semiconductor band gap can be reduced by residual strain, thus
363 leading to deformed potential [47,48]. Therefore, the low PL QY reveals that CdS core QDs suffer

364 from residual strain due to surface traps embedded within the nanocrystals. The narrow band gap
365 (2.07–2.11 eV) exhibited by the different-sized CdS/AgZnSe QDs (synthesized via method 1),
366 correlated precisely to the small difference in PL QY (48-51%). This suggests that suppression of
367 surface defect states in CdS QDs was with a very small margin across the core/alloyed shell QDs
368 size. However, a wider margin in defect state suppression was observed for CdS/AgZnSe QDs
369 synthesized via method 2, due to the wider difference in PL QY from 35% to 73%. Two important
370 features are the maximum PL QY of 73% and the precise correlation in the margin of difference
371 between the band gap and the PL QY. It is also noteworthy that the high PL QY implies much of
372 the surface defects were suppressed by the shell alloying process while the variation in PL QY
373 correlated precisely to the efficiency of surface defect suppression.

374

375 **4. Conclusions**

376 The passivation of CdS QDs with a new ternary alloyed AgZnSe shell layer was obtained via the
377 organometallic synthetic route. The band gap of CdS/AgZnSe core/alloyed shell QDs was tuned
378 across the visible region with the nanocrystals exhibiting varying PL QYs. We observed a precise
379 correlation in the margin of difference between the band gap of the QDs and the PL QY. The effect
380 of shell alloying was observed in the QDs growth morphology in which the QDs growth
381 transitioned from a homogeneous state to a heterogeneous state. Transition in the phase structure
382 of the QDs from a zinc blende diffraction pattern to a wurtzite diffraction pattern was also
383 observed. Generally, we have established that AgZnSe shell passivation on luminescent CdS QDs
384 suppressed interfacial defect states in the CdS core QDs with the degree of suppression dependent
385 on the size of the QDs derived from the finely-tuned synthetic fabrication strategy.

386

387 **Acknowledgement**

388 Financial support from the Water Research Council (WRC) project K5/2752, South Africa and the
389 University of Pretoria is gratefully acknowledged.

390

391 **Reference**

392 [1] T.V. Duncan, M.A. Mendez Polanco, Y. Kim and S.-J. Park, Improving the quantum yields of
393 semiconductor quantum dots through photoenhancement assisted by reducing agents, *J. Phys.*
394 *Chem. C*, 11 (2009) 7561–7566.

395 [2] A. Hassinen, I. Moreels, K. De Nolf, P.F. Smet, J.C. Martins and Z. Hens, Short-chain alcohols
396 strip X-type ligands and quench the luminescence of PbSe and CdSe Quantum dots,
397 acetonitrile does not, *J. Am. Chem. Soc.* 134 (2012) 20705–20712.

398 [3] M. Nasilowski, P. Spinicelli, G. Patriarche, B. Dubertret, Gradient CdSe/CdS quantum dots
399 with room temperature biexciton unity quantum yield, *Nano Lett.* 15 (2015) 3953–3958.

400 [4] P. Reiss, M. Protière, L. Li, Core/shell semiconductor nanocrystals, *Small* 5 (2009) 154–168.

401 [5] D.V. Talapin, J.-S. Lee, M.V. Kovalenko, E.V. Shevchenko, Prospects of colloidal
402 nanocrystals for electronic and optoelectronic applications. *Chem. Rev.* 110 (2010) 389–458.

403 [6] O. Chen, J. Zhao, V.P. Chauhan, J. Cui, C. Wong, D.K. Harris, H. Wei, H.-S. Han, D.
404 Fukumura, R.K. Jain, M.G. Bawendi, Compact high-quality CdSe–CdS core–shell
405 nanocrystals with narrow emission linewidths and suppressed blinking. *Nat. Mater.* 12 (2013)
406 445–451.

407 [7] C. Giansante, I. Infante, Surface traps in colloidal quantum dots: a combined experimental
408 and theoretical perspective, *J. Phys. Chem. Lett.* 8 (2017) 5209–5215.

- 409 [8] M. Nirmal, B.O. Dabbousi, M.G. Bawendi, J.J. Macklin, J.K. Trautman, T.D. Harris, L.E.
410 Brus, Fluorescence intermittency in single cadmium selenide nanocrystals, *Nature* 383 (1996)
411 802–804.
- 412 [9] A. Efros, M. Rosen, Random telegraph signal in the photoluminescence intensity of a single
413 quantum dot, *Phys. Rev. Lett.* 78 (1997) 1110–1113.
- 414 [10] Y. Altintas, M.Y. Talpur, M. Ünlü, E. Mutlugün, Highly efficient cd-free alloyed core/shell
415 quantum dots with optimized precursor concentrations, *J. Phys. Chem. C* 120 (2016)
416 7885–7892.
- 417 [11] J. Bang, J. Park, J.H. Lee, N. Won, J. Nam, J. Lim, B.Y. Chang, H.J. Lee, B. Vhon, J. Shin,
418 J.B. Park, .H. Choi, K. Cho, S.M. Park, T. Joo, S. Kim, ZnTe/ZnSe (core/shell) type-ii quantum
419 dots: their optical and photovoltaic properties, *Chem. Mater.* 22 (2010) 233–240.
- 420 [12] M.D. Tessier, D. Dupont, K. De Nolf, J. De Roo, Z. Hens, Economic and Size-tunable
421 synthesis of InP/ZnE (E = S, Se) colloidal quantum dots, *Chem. Mater.* 27 (2015) 4893–4898.
- 422 [13] W. Jiang, A. Singhal, J. Zheng, C. Wang, W.C.W. Chan, Optimizing the synthesis of red-
423 to near-ir-emitting CdS-capped CdTe_xSe_{1-x} alloyed quantum dots for biomedical imaging,
424 *Chem. Mater.* 18 (2006) 4845-4854.
- 425 [14] P. Tyagi, P. Kambhampati, Independent control of electron and hole localization in
426 core/barrier/shell nanostructures, *J. Phys. Chem. C*, 116 (2012) 8154–8160.
- 427 [15] M. Nasilowski, P. Spinicelli, G. Patriarche, B. Dubertret, Gradient CdSe/CdS quantum dots
428 with room temperature biexciton unity quantum yield. *Nano Lett.* 15 (2015) 3953–3958.
- 429 [16] M. Wang, M. Zhang, J. Qian, F. Zhao, L. Shen, G.D. Scholes, M.A. Winnik, Enhancing
430 the photoluminescence of polymer-stabilized CdSe/CdS/ZnS core/shell/shell and CdSe/ZnS

431 core/shell quantum dots in water through a chemical-activation approach, *Langmuir* 25 (2009)
432 11732–11740.

433 [17] W. Liu, H. Soo Choi, J.P. Zimmer, E. Tanaka, J.V. Frangioni, M. Bawendi, Compact
434 cysteine-coated CdSe(ZnCdS) quantum dots for in vivo applications, *J. Am. Chem. Soc.* 129
435 (2007) 14530-14531.

436 [18] K. Yu, S. Singh, N. Patrito, V. Chu, Effect of reaction media on the growth and
437 photoluminescence of colloidal CdSe nanocrystals, *Langmuir* 20 (2004) 11161-11168.

438 [19] R.E. Bailey, S. Nie, Alloyed semiconductor quantum dots: tuning the optical properties
439 without changing the particle size, *J. Am. Chem. Soc.* 125 (2003) 7100-7106.

440 [20] J. Quyang, C.I. Ratcliffe, D. Kingston, B. Wilkinson, J. Kuijper, X. Wu, J.A. Ripmeester,
441 K. Yu, Gradiently alloyed $Zn_xCd_{1-x}S$ colloidal photoluminescent quantum dots synthesized via
442 a noninjection one-pot approach, *J. Phys. Chem. C* 112 (2008) 4908-4919.

443 [21] R. Gui, A. Wan, H. Jin, H. Li, C. Zhou, Acetyl acetate-stabilized Mn^{2+} :CdS quantum
444 dots: Aqueous synthesis and reversible fluorescence tuned by redox reaction, *Mater. Lett.* 98
445 (2013) 190-193.

446 [22] R. Gui, X. An, H. Su, W. Shen, Z. Chen, X. Wang, A near-infrared-emitting CdTe/CdS
447 core/shell quantum dots-based OFF–ON fluorescence sensor for highly selective and sensitive
448 detection of Cd^{2+} , *Talanta* 94 (2012) 257-262.

449 [23] R. Gui, X. An, Layer-by-layer aqueous synthesis, characterization and fluorescence
450 properties of type-II CdTe/CdS core/shell quantum dots with near-infrared emission. *RSC*
451 *Adv.* 3 (2013) 20959-20969.

452 [24] M.V. Rama Krishna, R.A. Friesner, Quantum confinement effects in semiconductor
453 clusters, *J. Chem. Phys.* 95 (1991) 8309-8322.

- 454 [25] I. Hernandez-Calderon, II-VI Semiconductor Materials and Their Applications, (Ed.
455 Tamargo, M. C.), P136-138, Vol. 12 in Optoelectronic Properties of Semiconductors and
456 Superlattices; Manasreh, M. O., Ed.; Taylor & Francis Inc.: New York, 2002.
- 457 [26] A. I. Ekimov, I. A. Kudryavtsev, M. G. Ivanov, A.L. Efros, Spectra and decay kinetics of
458 radiative recombination in CdS microcrystals, *J. Lumin.* 46 (1990) 83-95.
- 459 [27] K. Gong, D.F. Kelley, Lattice strain limit for uniform shell deposition in zincblende
460 CdSe/CdS quantum dots, *J. Phys. Chem. Lett.* 6 (2015) 1559–1562.
- 461 [28] C.-C. Hung, S.-J. Ho, C.-W. Yeh, G.-H. Chen, J.-H. Huang, H.-S. Chen, Highly
462 luminescent dual-color-emitting alloyed $[\text{Zn}_x\text{Cd}_{1-x}\text{Se}_y\text{S}_{1-y}]$ quantum dots: investigation of
463 bimodal growth and application to lighting, *J. Phys. Chem. C* 121 (2017) 28373–28384.
- 464 [29] L.A. Swafford, L.A. Weigand, M.J. Bowers, J.R. McBride, J.L. Rapaport, T.L. Watt, S.K.
465 Dixit, L.C. Feldman, S.J. Rosenthal, Homogeneously alloyed $\text{CdS}_x\text{Se}_{1-x}$ nanocrystals:
466 synthesis, characterization, and composition/size-dependent band gap, *J. Am. Chem. Soc.* 128
467 (2006) 12299.
- 468 [30] Z. Pan, K. Zhao, J. Wang, H. Zhang, YY. Feng, X. Zhong, Near infrared absorption of
469 $\text{CdSe}_x\text{Te}_{1-x}$ alloyed quantum dot sensitized solar cells with more than 6% efficiency and high
470 stability, *ACS Nano* 7 (2013) 5215–5222.
- 471 [31] A. Kigel, M. Brumer, A. Sashchiuk, L. Amirav, E. Lifshitz, $\text{PbSe}/\text{PbSe}_x\text{S}_{1-x}$ core-alloyed
472 shell nanocrystals, *Mater. Sci. Eng., C* 25 (2005) 604-608.
- 473 [32] H. Jin, R. Gui, Z. Wang, J. Xia, M. Yang, F. Zhang, S. Bi, Facile fabrication of water-
474 dispersible AgInS_2 quantum dots and mesoporous AgInS_2 nanospheres with visible
475 photoluminescence, *RSC Adv.* 5 (2015) 68287-68292.

- 476 [33] P. Yang, M. Ando, N. Murase, Highly luminescent CdSe/Cd_xZn_{1-x}S quantum dots coated
477 with thickness-controlled SiO₂ shell through silanization, *Langmuir* 27 (2011) 9535–9540.
- 478 [34] K. Boldt, N. Kirkwood, G.A. Beane, P. Mulvaney, Synthesis of highly luminescent and
479 photo-stable, graded shell CdSe/Cd_xZn_{1-x}S nanoparticles by in situ alloying, *Chem. Mater.* 25
480 (2013) 4731–4738.
- 481 [35] S.M. Fairclough, E.J. Tyrrell, D.M. Graham, P.J.B. Lunt, S.J.O. Hardman, A. Pietzsch, F.
482 Hennies, J. Moghal, W.R. Flavell, A.A.R. Watt, J.M.J. Smith, Growth and characterization of
483 strained and alloyed Type-II ZnTe/ZnSe core–shell nanocrystals, *Phys. Chem. C* 16 (2012)
484 26898–26907.
- 485 [36] W.K. Bae, L.A. Padilha, Y.-S. Park, H. McDaniel, I. Robel, J.M. Pietryga, V.I. Klimov,
486 Controlled alloying of the core-shell interface in CdSe/CdS quantum dots for suppression of
487 Auger recombination, *ACS Nano* 7 (2013) 3411–3419.
- 488 [37] O. Adegoke, K. Takemura, E.Y. Park, Plasmonic oleylamine-capped gold and silver
489 nanoparticle-assisted synthesis of luminescent alloyed CdZnSeS quantum dots, *ACS Omega* 3
490 (2018) 135-1366.
- 491 [38] J. Quyang, C.I. Ratcliffe, D. Kingston, B. Wilkinson, J. Kuijper, X. Wu, J.A. Ripmeester,
492 K. Yu, Gradiently alloyed Zn_xCd_{1-x}S colloidal photoluminescent quantum dots synthesized via
493 a noninjection one-pot approach, *J. Phys. Chem. C* 112 (2008) 4908-4919.
- 494 [39] B.O. Dabbousi, . Rodriguez-Viejo, F.V. Mikulec, J.R. Heine, H. Mattoussi, R. Ober, K.F.
495 Jensen, M.G. Bawendi, (CdSe)ZnS core-shell quantum dots: synthesis and characterization of
496 a size series of highly luminescent nanocrystallites, *J. Phys. Chem. B* 101 (1997) 9463-9475.
- 497 [40] D.V. Talapin, I. Mekis, S. Götzinger, A. Kornowski, O. Benson, H. Weller, CdSe/CdS/ZnS
498 and CdSe/ZnSe/ZnS core-shell-shell nanocrystals, *J. Phys. Chem. B* 108 (2004) 18826-18831.

- 499 [41] P.T.K. Chin, C. de Mello Donega, S.S. van Bavel, S.C.J. Meskers, N.A.J.M. Sommerdijk,
500 R.A.J. Janssen, Highly luminescent CdTe/CdSe colloidal heteronanocrystals with temperature-
501 dependent emission color, *J. Am. Chem. Soc.* 129 (2007) 14880-14886.
- 502 [42] N.T.K. Thanh, N. Maclean, S. Mahiddine, Mechanisms of nucleation and growth of
503 nanoparticles in solution, *Chem. Rev.* 114 (2014) 7610–7630.
- 504 [43] F.; Garcia-Santamaría, S. Brovelli, R. Viswanatha, J.A. Hollingsworth, H. Htoon, S.A.
505 Crooker, V.I. Klimov, Breakdown of volume scaling in Auger recombination in CdSe/CdS
506 heteronanocrystals: the role of the core-shell interface, *Nano Lett.* 11 (2011) 687–693.
- 507 [44] G.E. Cragg, A.L. Efros, Suppression of auger processes in confined structures, *Nano Lett.*
508 10 (2009) 313–317.
- 509 [45] F. Comas, N. Studart, G.E. Marques, Optical phonons in semiconductor quantum rods,
510 *Solid State Commun.* 130 (2004) 477–480.
- 511 [46] H. Lange, M. Artemyev, U. Woggon, C. Thomsen, Geometry dependence of the phonon
512 modes in CdSe nanorods, *Nanotechnology* 20 (2009) 045705.
- 513 [47] J. Kim, M.V. Fischetti, Electronic band structure calculations for biaxially strained Si, Ge,
514 and III-V Semiconductors. *J. Appl. Phys.* 108 (2010) 013710.
- 515 [48] J. Kim, M.V. Fischetti, S. Aboud, Structural, electronic, and transport properties of silicane
516 nanoribbons. *Phys. Rev. B* 86 (2012) 205323.

517

518

519

520

521

522 **Table 1.** Summary of the photophysical properties of the different-sized CdS core and
523 CdS/AgZnSe QDs.

QDs- λ_{Emi} (nm)	λ_{Abs} (nm)	FWHM (nm)	Band gap (eV)	PL QY (%)
CdS ₄₇₁	458	20	2.64	16
CdS ₄₇₈	471	26	2.60	4
CdS ₄₈₁	476	33	2.58	8
^a CdS/AgZnSe ₅₈₈	464	41	2.11	48
^b CdS/AgZnSe ₅₉₁	449	34	2.10	73
^a CdS/AgZnSe ₅₉₃	468	42	~2.10	50
^a CdS/AgZnSe ₅₉₉	473	40	2.07	49
^a CdS/AgZnSe ₆₀₁	477	45	~2.07	51
^b CdS/AgZnSe ₆₀₂	473	39	2.06	35
^b CdS/AgZnSe ₆₁₂	481	40	2.03	42

524 ^a Method 1 synthesis

525 ^b Method 2 synthesis

526

527

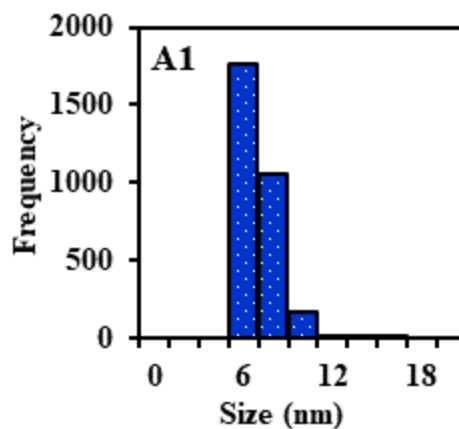
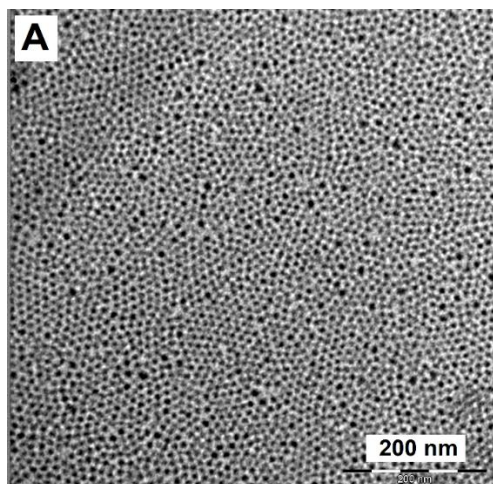
528

529

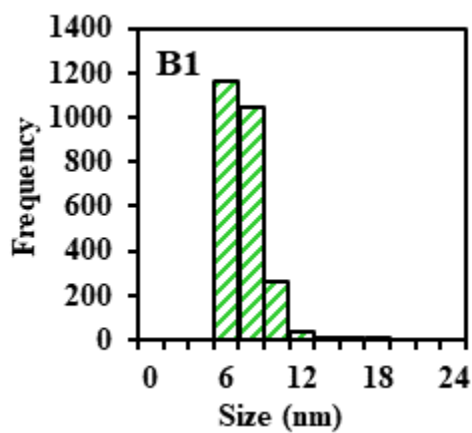
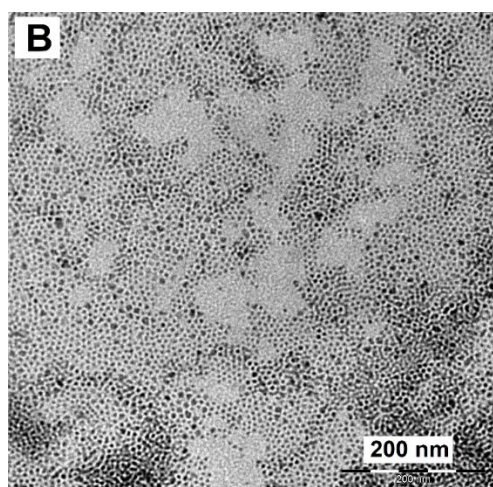
530

531

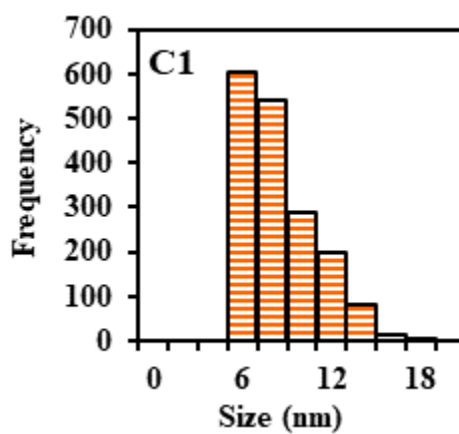
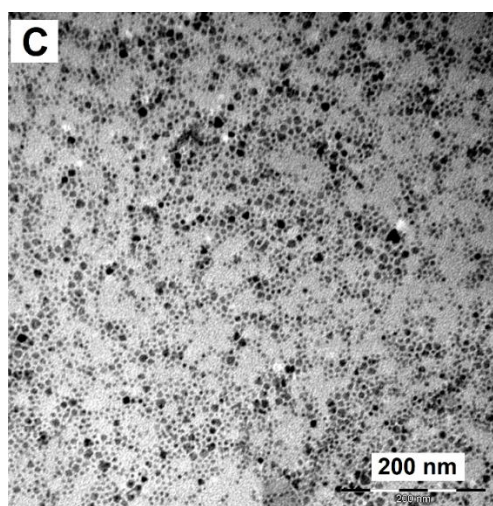
532



533

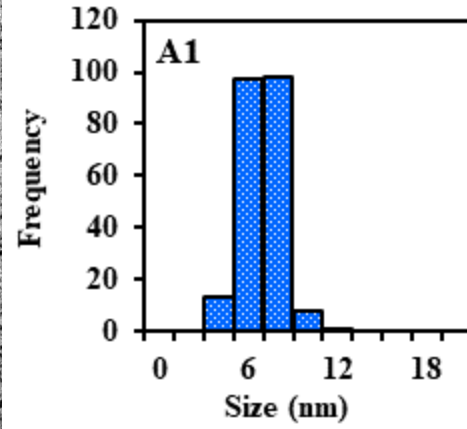
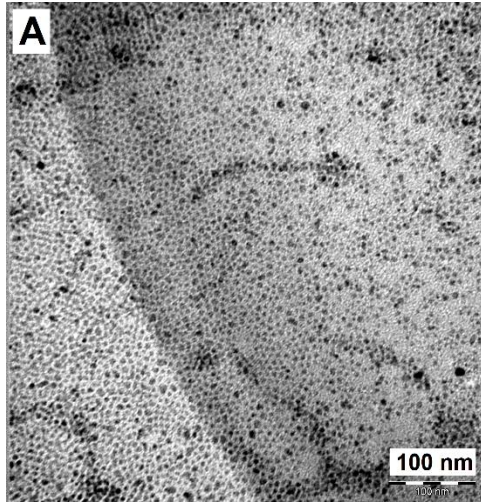


534

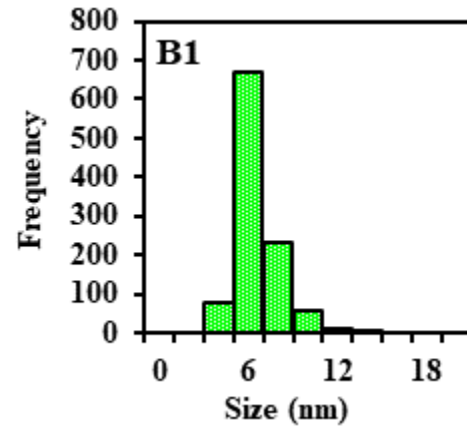
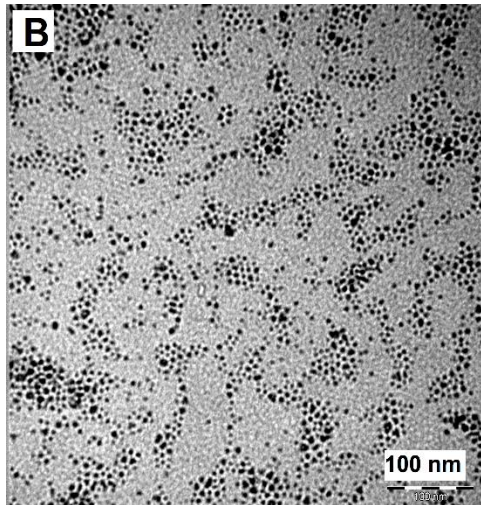


535 **Fig. 1.** TEM images (A, B and C) and average particle size distribution (A1, B1 and C1) of CdS
536 core QDs.

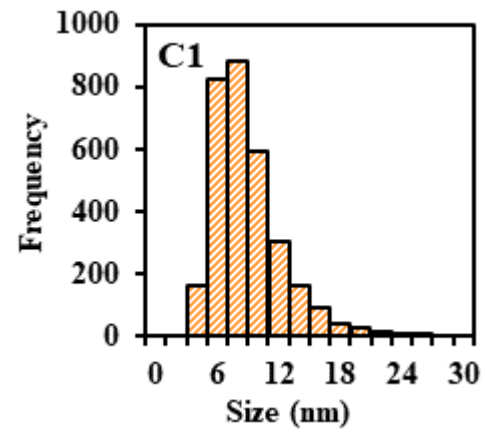
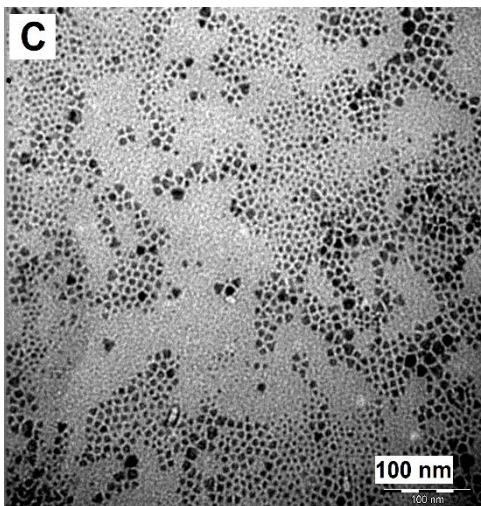
537



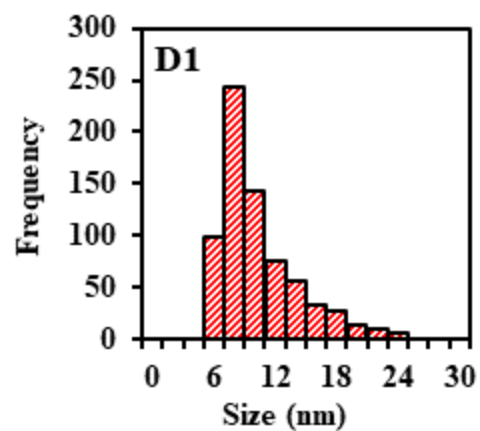
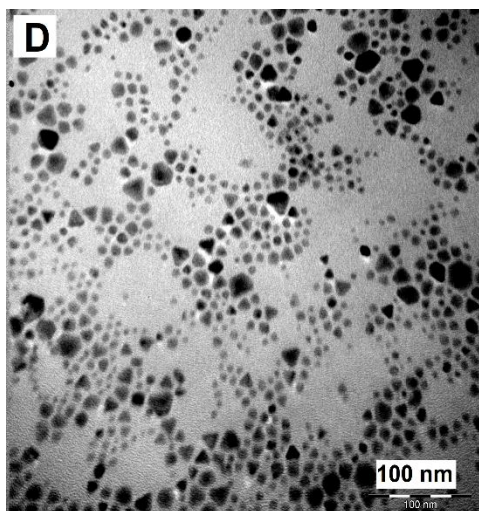
538



539



540



541

542 **Fig. 2.** TEM images (A, B, C and D) and average particle size distribution (A1, B1, C1 and D1)

543 of CdS/AgZnSe core/alloyed shell QDs synthesized via method 1.

544

545

546

547

548

549

550

551

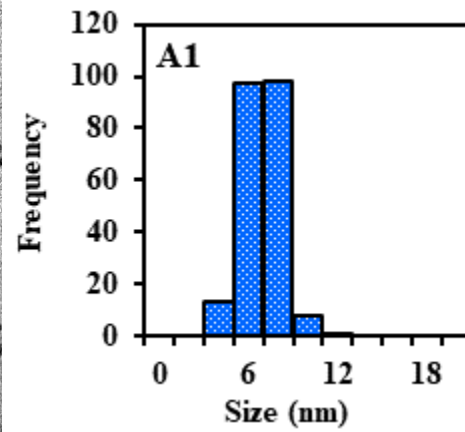
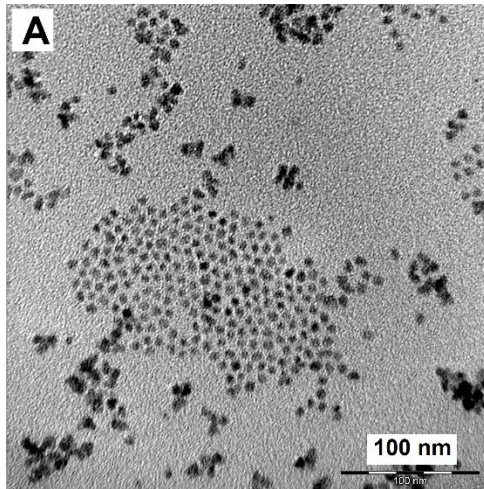
552

553

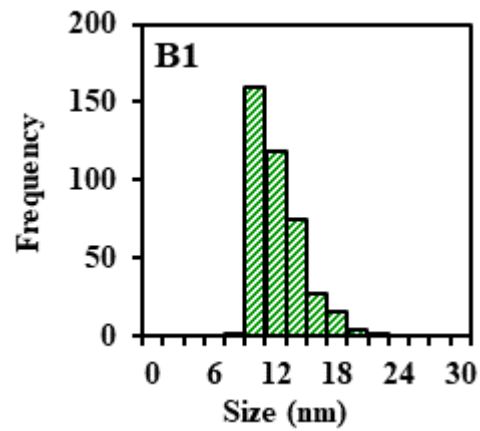
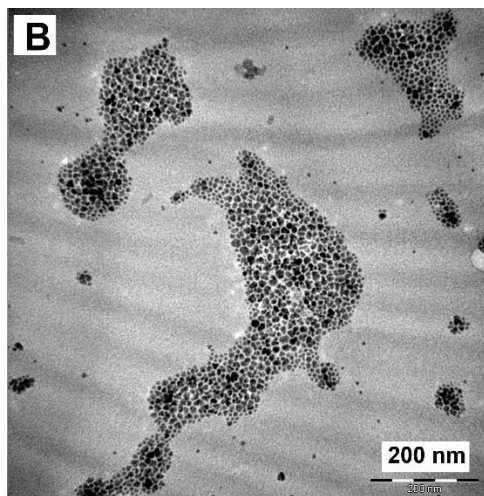
554

555

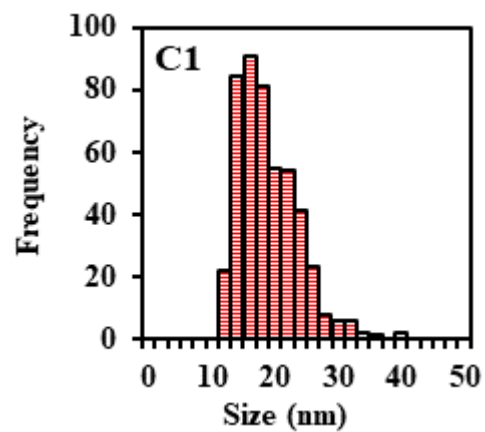
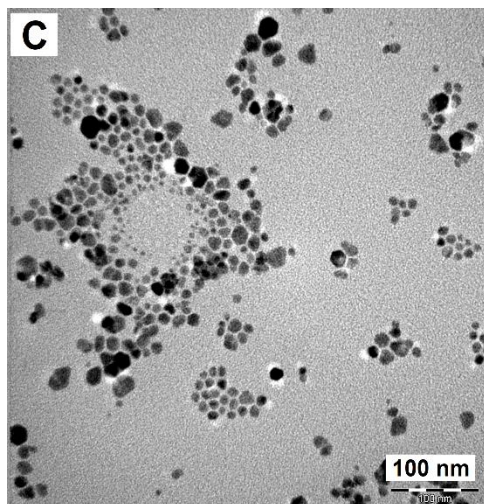
556



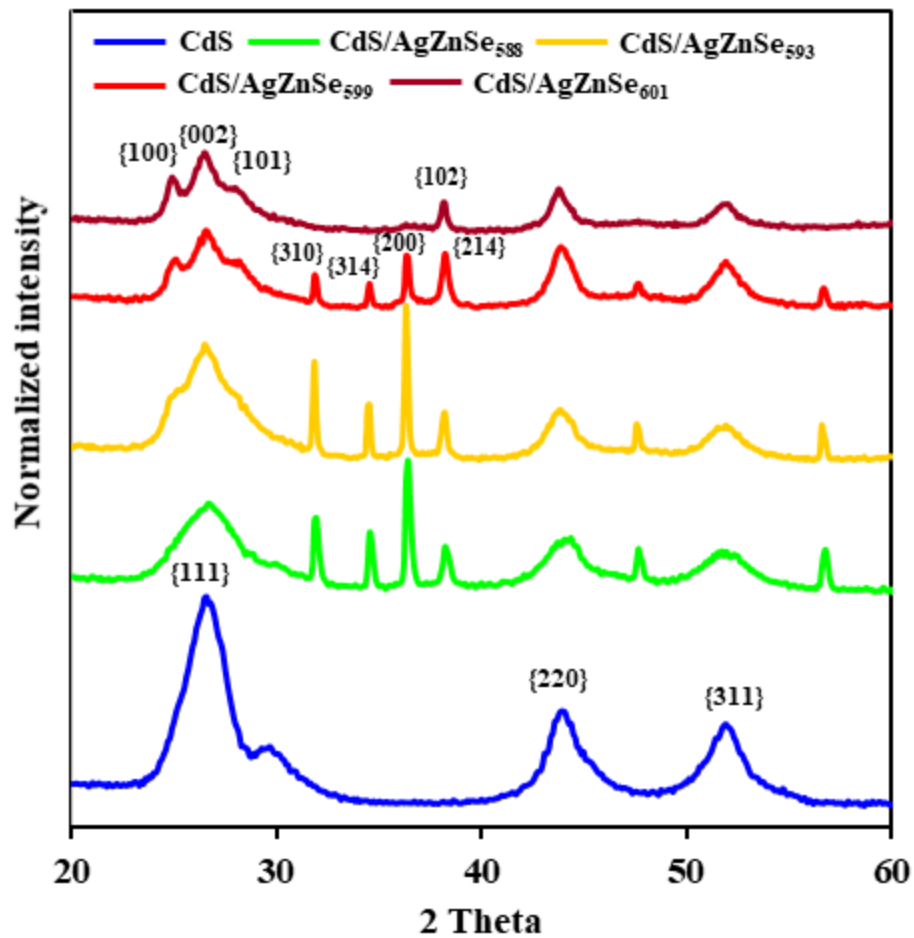
557



558

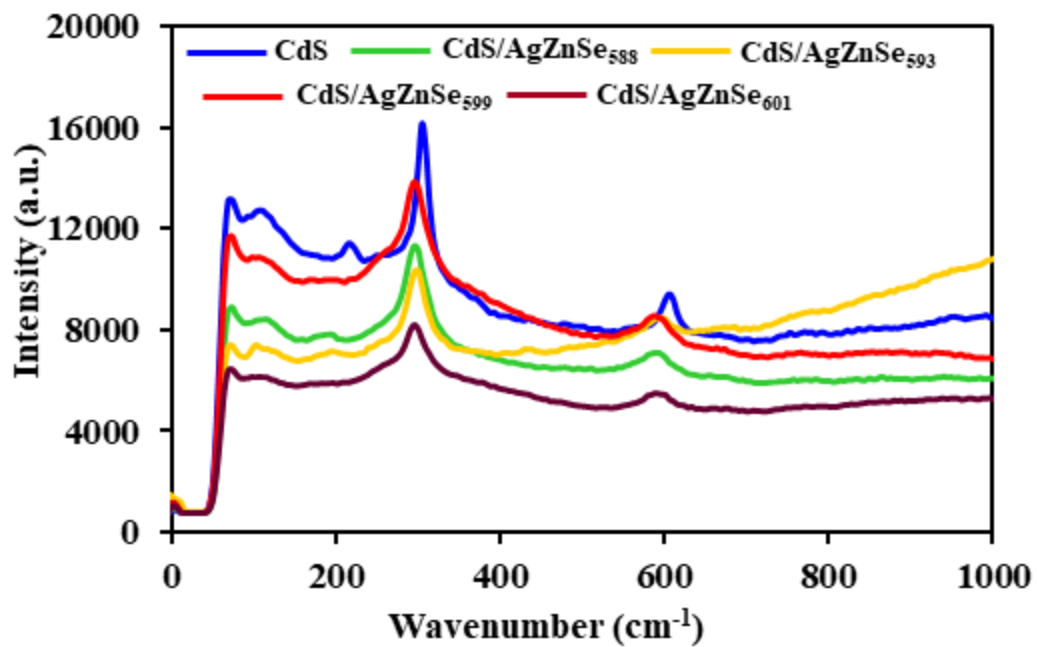


559 **Fig. 3.** TEM images (A, B and C) and average particle size distribution (A1, B1 and C1) of
560 CdS/AgZnSe core/alloyed shell QDs synthesized via method 2.



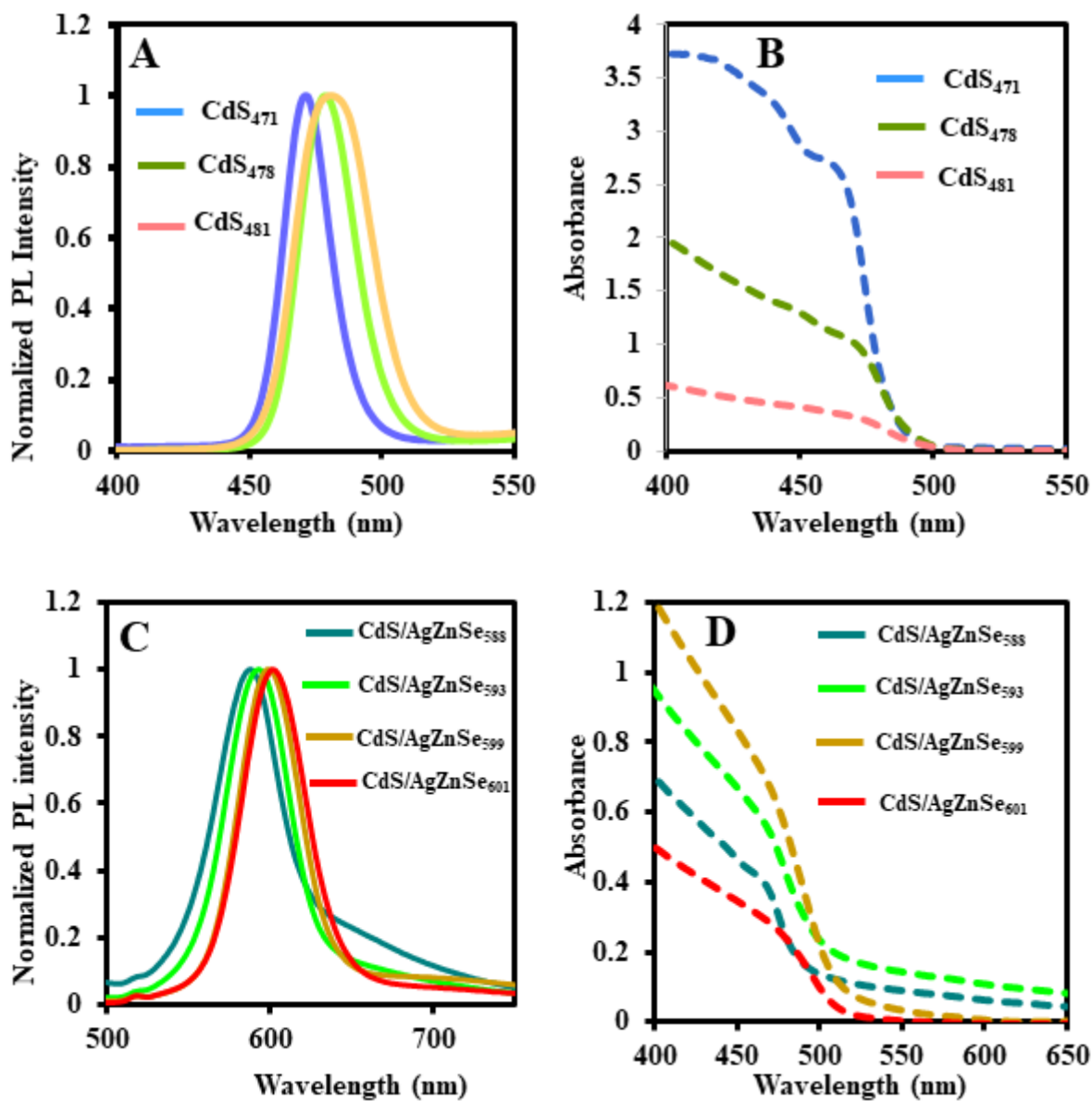
561
 562 **Fig. 4.** PXRD plots of CdS, CdS/AgZnSe₅₈₈, CdS/AgZnSe₅₉₃, CdS/AgZnSe₅₉₉ and CdS/AgZnSe₆₀₁
 563 QDs.

564
 565
 566
 567
 568
 569
 570
 571



572
 573 **Fig. 5.** Raman spectra of CdS, CdS/AgZnSe₅₈₈, CdS/AgZnSe₅₉₃, CdS/AgZnSe₅₉₉ and
 574 CdS/AgZnSe₆₀₁ QDs.

575
 576
 577
 578
 579
 580



581

582

583 **Fig. 6.** PL and UV/vis absorption spectra of the different sized CdS (A and B) and CdS/AgZnSe
 584 core/alloyed shell QDs (C and D) synthesized via method 1.

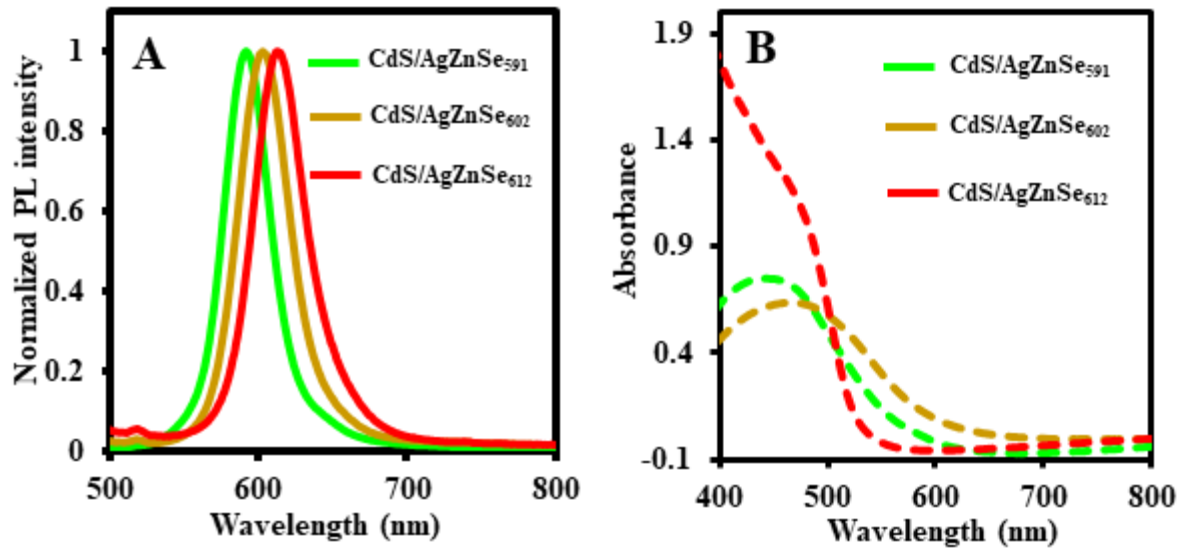
585

586

587

588

589



590
 591 **Fig. 7.** PL (A) and UV/vis absorption (B) spectra of the different sized and CdS/AgZnSe
 592 core/alloyed shell QDs synthesized via method 2.

593
 594
 595
 596
 597
 598
 599
 600
 601
 602
 603
 604